

^8He and ^9Li cluster structures in light nuclei

Naoyuki Itagaki,¹ Tokuro Fukui,¹ Junki Tanaka,² and Yuma Kikuchi³

¹*Yukawa Institute for Theoretical Physics, Kyoto University,
Kitashirakawa Oiwake-Cho, Kyoto 606-8502, Japan*

²*RIKEN Nishina Center for Accelerator-Based Science, 2-1 Hirosawa, Wako, Saitama 351-0198, Japan*

³*Tokuyama College of Technology, Gakuendai, Shunan, Yamaguchi 745-8585, Japan*

(Dated: May 1, 2020)

The possibility of the ^8He and ^9Li clusters in atomic nuclei is discussed. Until now most of the clusters in the conventional models have been limited to the closures of the three-dimensional harmonic oscillators, such as ^4He , ^{16}O , and ^{40}Ca . In the neutron-rich nuclei, however, the neutron to proton ratio is not unity, and it is worthwhile to think about more neutron-rich objects with $N > Z$ as the building blocks of cluster structures. Here the nuclei with the neutron number six, which is the subclosure of the $p_{3/2}$ subshell of the jj -coupling shell model, are assumed to be clusters, and thus we study the ^8He and ^9Li cluster structures in ^{16}Be ($^8\text{He}+^8\text{He}$), ^{17}B ($^8\text{He}+^9\text{Li}$), ^{18}C ($^9\text{Li}+^9\text{Li}$), and ^{24}C ($^8\text{He}+^8\text{He}+^8\text{He}$). Recent progress of the antisymmetrized quasi cluster model (AQCM) enables us to utilize jj -coupling shell model wave functions as the clusters rather easily. It is shown that the $^8\text{He}+^9\text{Li}$ and $^9\text{Li}+^9\text{Li}$ cluster configurations cover the lowest shell-model states of ^{17}B and ^{18}C , respectively. To predict the cluster states with large relative distances, we increase the expectation value of the principal quantum numbers by adding the nodes to the lowest states under the condition that the total angular momentum is unchanged (equal to $J^\pi = 0$). As a result, developed cluster states are obtained around the corresponding threshold energies. The rotational band structure of ^{24}C , which reflect the symmetry of equilateral triangular configuration (D_{3h} symmetry) of three ^8He clusters, also appears around the threshold energy.

I. INTRODUCTION

The ^4He nuclei have been known as α clusters, which can be subsystems in some of light nuclei [1, 2]. The binding energy of ^4He is quite large in the light mass region, and on the contrary, the relative interaction between ^4He nuclei is weak. Therefore each ^4He can be considered as a subunit called α cluster. The candidates for α cluster structures have been discussed for many years [3], including the second 0^+ state of ^{12}C with a developed three- α cluster structure called Hoyle state [4].

In most of the conventional cluster models, the clusters have been limited to the closure of the three-dimensional harmonic oscillator, such as ^4He , ^{16}O , and ^{40}Ca , where the contribution of the non-central interactions (spin-orbit and tensor interactions) vanishes. However, in the nuclear systems, the symmetry of the jj -coupling shell model is more important, where the contribution of the spin-orbit interaction breaks the symmetry of the three-dimensional harmonic oscillator, and the subclosure of j -upper shells, $f_{7/2}$, $g_{9/2}$, and $h_{11/2}$, is essential in explaining the observed magic numbers of 28, 50, and 126 [5]. Indeed this spin-orbit interaction is also known as a driving force in breaking the α clusters [6]. Therefore, it would be meaningful to extend the traditional definition of the clusters; different objects could be candidates for the clusters.

Now we focus on the neutron-rich nuclei, which have been the main subject of nuclear structure physics for decades. In neutron-rich nuclei, the ratio of proton number and neutron number deviates from unity. Therefore, it is worthwhile to consider neutron-rich clusters whose neutron numbers correspond to the subclosure of the j -

upper orbits of the jj -coupling shell model, where the spin-orbit interaction works attractively. Here we discuss the possibility that nuclei with the neutron number six, which is the subclosure of the j -upper shell, $p_{3/2}$, can be clusters. Previously we have discussed the possibility of ^{14}C cluster as building blocks of medium-heavy nuclei [7], whose proton number (six) corresponds to the subclosure of $p_{3/2}$. As the next step, we show the possibility of the ^8He (two protons and six neutrons) and ^9Li (three protons and six neutrons) cluster structures in ^{16}Be ($^8\text{He}+^8\text{He}$), ^{17}B ($^8\text{He}+^9\text{Li}$), ^{18}C ($^9\text{Li}+^9\text{Li}$), and ^{24}C ($^8\text{He}+^8\text{He}+^8\text{He}$).

It has been studied that Be isotopes are well described as two α clusters with valence neutrons. Here, the molecular-orbit structure of the valence neutrons, where each valence neutron rotates not around only one α cluster but around two α clusters, has been found to be important [8–14]. Thus $^4\text{He}+^6\text{He}$ and $^5\text{He}+^5\text{He}$ configurations mix for instance in ^{10}Be . However, it is also known that some of the excited states of ^{12}Be has not the molecular-orbit but the atomic-orbit structure of the $^6\text{He}+^6\text{He}$ or $^4\text{He}+^8\text{He}$ configuration [13, 15, 16], where each valence neutron sticks to one of the α clusters. It should be stressed that the appearance of both molecular and atomic-orbit structures in Be isotopes including ^{16}Be has been systematically studied with generalized two-center cluster model (GTCM) [17]. In the present study, we treat ^8He as a cluster based on the atomic-orbit picture and go beyond the Be isotopes.

The nucleus ^8He is the dripline nucleus of the He isotopes and has a neutron-halo structure. The valence neutrons are known to have an intermediate character of di-neutron structure and independent particle mo-

tion [18, 19]. Nevertheless, the two-neutron separation energy of 2.12 MeV is larger than that of ${}^6\text{He}$ (0.98 MeV), and here we simplify it with the jj -coupling shell model configuration with the ${}^4\text{He}$ core and consider this nucleus as a subunit.

We also introduce ${}^9\text{Li}$ cluster and discuss ${}^{17}\text{B}$ (${}^8\text{He}+{}^9\text{Li}$) and ${}^{18}\text{C}$ (${}^9\text{Li}+{}^9\text{Li}$). The neutron separation energy of ${}^9\text{Li}$ is 4.06 MeV and not very large, but this is larger than ${}^8\text{He}$ and various ${}^9\text{Li}+n+n$ models have been applied to ${}^{11}\text{Li}$ so far [20]. Although the structure of ${}^9\text{Li}$ itself is a subject to be carefully investigated, here we simplify it as a cluster using the lowest shell-model configuration as in the ${}^8\text{He}$ case and discuss the cluster structure in the heavy nuclei. The two-center-like deformation was predicted in ${}^{17}\text{B}$ with the ${}^8\text{He}+{}^9\text{Li}$ configuration [21], and we further investigate the appearance of more developed cluster states around the threshold energy.

Recently, the wave functions of the jj -coupling shell model can be easily prepared by starting with the cluster model. Indeed, the antisymmetrized quasi cluster model (AQCM) proposed in Refs. [7, 22–32] allows smooth transformation of the cluster model wave functions to the jj -coupling shell model ones, as well as the incorporation of the effects of the spin-orbit interaction, which is absent in many of the traditional α cluster models. Therefore, now we can utilize jj -coupling shell model wave functions as the building blocks of the cluster structure. In this article, we introduce ${}^8\text{He}$ and ${}^9\text{Li}$ clusters using AQCM.

In this paper, we discuss that the ${}^8\text{He}+{}^9\text{Li}$ and ${}^9\text{Li}+{}^9\text{Li}$ cluster configurations cover the lowest shell-model states of ${}^{17}\text{B}$ and ${}^{18}\text{C}$, respectively. Also we show the appearance of developed cluster states around the corresponding threshold energies by orthogonalizing to the lowest states. In addition, the rotational band structure of ${}^{24}\text{C}$, which reflect the symmetry of equilateral triangular configuration (D_{3h} symmetry) of three ${}^8\text{He}$ clusters, will be presented. Although these cluster states are above the neutron-threshold energies, they appear around the cluster-threshold energies.

This paper is organized as follows. The framework of AQCM is described in Sec. II. The results are shown in Sec. III, where ${}^8\text{He}+{}^8\text{He}$ structure in ${}^{16}\text{Be}$, ${}^9\text{Li}+{}^8\text{He}$ structure in ${}^{17}\text{B}$, ${}^9\text{Li}+{}^9\text{Li}$ structure in ${}^{18}\text{C}$, and three ${}^8\text{He}$ structure in ${}^{24}\text{C}$ are discussed in **A.**, **B.**, **C.**, and **D.**, respectively. The conclusions are presented in Sec. IV.

II. FRAMEWORK

A. wave function

We analyze the ${}^8\text{He}$ and ${}^9\text{Li}$ cluster structures within the framework of AQCM. The neutrons of these clusters correspond to the subclosure of $p_{3/2}$ in the jj -coupling shell model, which can be easily prepared starting from the cluster model; AQCM allows the smooth transformation of the cluster model wave functions to the jj -

coupling shell model ones.

In AQCM, each single particle is described by a Gaussian form as in many other cluster models including the Brink model [1],

$$\phi = \left(\frac{2\nu}{\pi}\right)^{\frac{3}{4}} \exp\left[-\nu(\mathbf{r}-\boldsymbol{\zeta})^2\right] \chi, \quad (1)$$

where the Gaussian center parameter $\boldsymbol{\zeta}$ is related to the expectation value of the position of the nucleon, and χ is the spin-isospin part of the wave function. For the size parameter ν , here we use $\nu = 0.23 \text{ fm}^{-2}$.

The Slater determinant Φ_{SD} is constructed from these single particle wave functions by antisymmetrizing them, which is projected to the eigen states of the angular momenta by numerical integration,

$$\Phi_{MK}^J = \frac{2J+1}{8\pi^2} \int d\Omega D_{MK}^J * R(\Omega) \Phi_{SD}. \quad (2)$$

Here D_{MK}^J is Wigner D-function and $R(\Omega)$ is the rotation operator for the spatial and spin parts of the wave function. This integration over the Euler angle Ω is numerically performed.

Next we focus on the Gaussian center parameters $\{\boldsymbol{\zeta}\}$. As in other cluster models, here four single particle wave functions with different spin and isospin sharing a common $\boldsymbol{\zeta}$ value correspond to an α cluster. This cluster wave function is transformed to jj -coupling shell model based on the AQCM. When the original value of the Gaussian center parameter $\boldsymbol{\zeta}$ is \mathbf{R} , which is real and related to the spatial position of this nucleon, it is transformed by adding the imaginary part as

$$\boldsymbol{\zeta} = \mathbf{R} + i\Lambda \mathbf{e}^{\text{spin}} \times \mathbf{R}, \quad (3)$$

where \mathbf{e}^{spin} is a unit vector for the intrinsic-spin orientation of this nucleon. The control parameter Λ is associated with the breaking of the cluster, and with a finite value of Λ , the two nucleons with opposite spin orientations have the $\boldsymbol{\zeta}$ values, which are complex conjugate with each other. This situation corresponds to the time-reversal motion of two nucleons.

For the description of ${}^8\text{He}$, at first, di-nucleon clusters are prepared; in each di-nucleon cluster, two nucleons with opposite spin and same isospin are sharing a common value for the Gaussian center parameters. For the proton part, one di-proton cluster is placed at the origin, which corresponds to the lowest $(0s)^2$ configuration of the shell-model. For the neutron part, three di-neutron clusters with equilateral triangular configuration and small distance (R) between them are introduced, and the imaginary parts of the Gaussian center parameters are given by setting $\Lambda = 1$ in Eq. (3), which correspond to the subclosure of the $p_{3/2}$ shell [22, 27]. In the actual calculations, R is set to 0.1 fm. This ${}^8\text{He}$ cluster is the eigen state of $J^\pi = 0^+$, and projection of the total angular momentum of the total system just gives the orbital angular momentum of the relative motion in the case of ${}^{16}\text{Be}$ (${}^8\text{He}-{}^8\text{He}$).

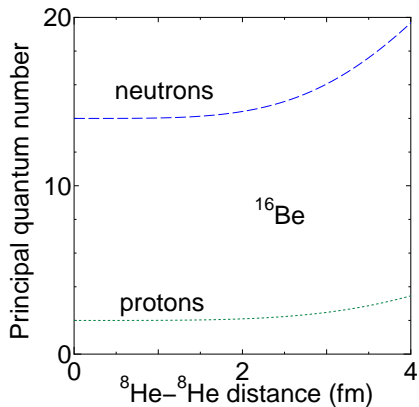


FIG. 1. Expectation value for the principal quantum number of the harmonic oscillator (n) for the 0^+ state of ^{16}Be as a function of the distance between two ^8He clusters. Dotted and dashed lines are results for the protons and neutrons, respectively.

For ^9Li , one more proton in the $p_{3/2}$ orbit is added. The Gaussian center parameter of the proton in the $p_{3/2}$ orbit is introduced in the following way. The proton is placed with a small x component ($R = 0.1$ fm), and the y component is given following Eq. (3), where the spin orientation is defined along the z axis (corresponding to spin-up or spin-down proton). This ^9Li cluster is the eigen state of $J^\pi = 3/2^-$.

For the calculations of ^{16}Be , ^{17}B , and ^{18}C , we translationally shift the Gaussian center parameters of the ^8He and ^9Li clusters and place them on the z axis. For ^{24}C , three ^8He clusters are placed to have an equilateral triangular shape.

B. Hamiltonian

The Hamiltonian consists of the kinetic energy and potential energy terms. The potential energy has central, spin-orbit, and Coulomb parts. For the central part, the Tohsaki interaction (F1 parameter set) [33] is adopted, which has finite range three-body nucleon-nucleon interaction terms in addition to two-body terms. This interaction is designed to reproduce both saturation properties and scattering phase shifts of two α clusters. For the spin-orbit part, that of the G3RS interaction [34], which is a realistic interaction originally developed to reproduce the nucleon-nucleon scattering phase shifts, is adopted. The combination of these two has been investigated in detail in Refs. [31, 32].

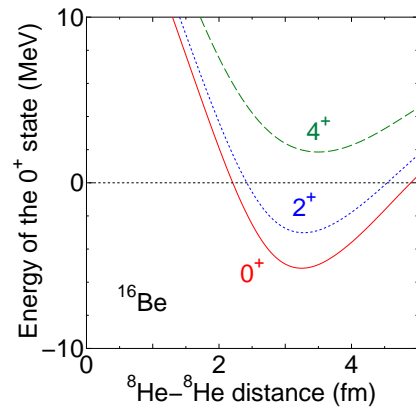


FIG. 2. Energy curves for ^{16}Be measured from the two- ^8He threshold as a function of the distance between two ^8He clusters. Solid, dotted, and dashed lines correspond to the 0^+ , 2^+ , and 4^+ states, respectively.

III. RESULTS

A. $^8\text{He}+^8\text{He}$ cluster structure in ^{16}Be

We start the discussion with the $^8\text{He}+^8\text{He}$ cluster structure in ^{16}Be . The dripline nucleus of the Be isotopes is ^{14}Be , thus ^{16}Be is located outside the neutron dripline. Experimentally, the two-neutron separation energy is -1.35 MeV (unbound), but the ground state is lower than the $^8\text{He}+^8\text{He}$ threshold by 5.77 MeV.

First, we show that the $^8\text{He}+^8\text{He}$ model space covers the lowest shell-model configuration of ^{16}Be . The expectation value for the principal quantum number of the harmonic oscillator (n) for the 0^+ state of ^{16}Be is shown in Fig. 1 as a function of the distance between two ^8He clusters. The dotted and dashed lines represent the results for the protons and neutrons, respectively, which converge to 2 and 14 at small relative distances. These values agree with the ones for the lowest shell-model configuration; for the protons, two are in the lowest $0s$ -shell and two are in the p -shell ($2 \times 1 = 2$), and for the neutrons, two are in the lowest $0s$ -shell, six are in the p -shell, and four are in the sd -shell ($6 \times 1 + 4 \times 2 = 14$). Therefore, the lowest shell-model configuration is included in the model space. With increasing the relative distance between the two ^8He clusters, the components of higher shells mix, and the n value rapidly increases.

Next, the energy curves for ^{16}Be measured from the two- ^8He threshold is shown in Fig. 2 as a function of the distance between two ^8He clusters. The solid, dotted, and dashed lines are the results for the 0^+ , 2^+ , and 4^+ states, respectively. It can be seen that the optimal energy for the 0^+ state is obtained with the relative distance of ~ 3 fm. This means that the lowest energy is obtained not at the limit of the shell-model, and clustering is found to be important, which is indeed higher shell mixing in terms of the shell model. Although we do not have adjustable parameters, the lowest energy is

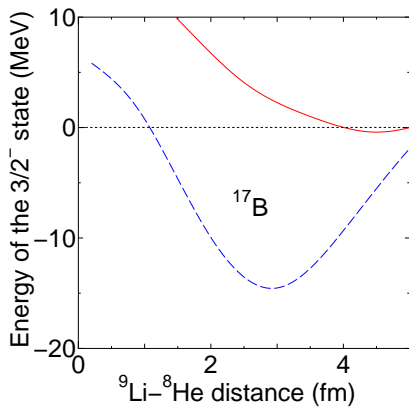


FIG. 3. Energy for the $3/2^-$ state of ^{17}B measured from the $^9\text{Li}-^8\text{He}$ threshold as a function of the distance between ^9Li and ^8He (dashed line). Energy curve for the $3/2^-$ state orthogonal to the state having the optimal distance of 3 fm (solid line).

close to the experimental binding energy of 5.77 MeV. Despite this binding energy, which is enough large, the optimal distance is large owing to the Pauli blocking effect at short relative distances between two ^8He clusters, and developed cluster structure appears. For the 2^+ and 4^+ states, the optimal distances are slightly larger than the one for the 0^+ state due to the centrifugal force.

B. $^9\text{Li}+^8\text{He}$ cluster structure in ^{17}B

We add one proton and show the result of $^9\text{Li}-^8\text{He}$ cluster configuration in ^{17}B . The dashed line in Fig. 3 shows the energy for the lowest $3/2^-$ state of ^{17}B measured from the $^9\text{Li}-^8\text{He}$ threshold as a function of the distance between ^9Li and ^8He . Experimentally, the ^{17}B nucleus is bound from the $^9\text{Li}+^8\text{He}$ threshold by 12.86 MeV. It is not perfect but the obtained lowest energy is fairly close to this value. Similarly to the $^8\text{He}+^8\text{He}$ case, despite this large binding energy, the relative distance at the optimal energy is also large owing to the Pauli blocking effect at short relative distances between the two clusters. In this calculation, ^9Li and ^8He clusters are placed on the z -axis, while the last proton in ^9Li stays on the perpendicular plane, and there is no additional excitation to higher shells for this proton when the ^8He cluster approaches. Therefore, again the lowest shell-model configuration of ^{17}B is included in the model space.

The energy curve for the $3/2^-$ state orthogonal to the lowest state (relative distance of 3 fm) is shown as the solid line. It is intriguing to see that the energy minimum point appears around the threshold energy with a very large relative distance of 4 fm. The appearance of very developed cluster structure around the threshold is expected, and adding neutrons to this state and investigating the molecular-orbital structure would be performed in the near future.

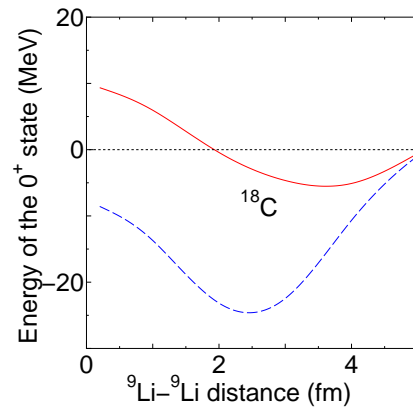


FIG. 4. Energy for the 0^+ state of ^{18}C measured from the two- ^9Li threshold as a function of the distance between two ^9Li clusters (dashed line). Energy curve for the 0^+ state orthogonal to the state having the optimal distance of 2.5 fm (solid line).

C. $^9\text{Li}+^9\text{Li}$ cluster structure in ^{18}C

For ^{18}C , we introduce a $^9\text{Li}+^9\text{Li}$ model. Here the spin directions of the valence protons in two ^9Li clusters are introduced to be anti-parallel, and two valence protons occupy the time-reversal orbits. Thus again the model space covers the lowest shell-model configuration of ^{18}C . The dashed line in Fig. 4 shows the energy for the lowest 0^+ state of ^{18}C measured from the two- ^9Li threshold as a function of the distance between two ^9Li clusters. The optimal energy is obtained around the relative distance of 2.5 fm. Experimentally, the ground state of ^{18}C is lower than the two- ^9Li threshold by 24.99 MeV. Again, although we do not use any adjustable parameter, the obtained optimal energy is fairly close to this value.

The solid line in Fig. 4 shows the energy curve for the 0^+ state orthogonal to the lowest state with the relative distance of 2.5 fm. Again, the appearance of the significantly clusterized state around the threshold energy with the relative distance of ~ 4 fm is expected. The intrinsic densities of this state on the xz -plane ($y = 0$) with the relative distance of 4 fm are represented by Fig. 5(a) and Fig. 5(b) for protons and neutrons, respectively. As a future work, adding neutrons to this state would be interesting.

D. three ^8He cluster structure in ^{24}C

Finally, we discuss the three ^8He cluster structure in ^{24}C . The dripline nucleus of the C isotopes is ^{22}C and hence ^{24}C is beyond the neutron dripline. Nevertheless, the three- ^8He states are shown to appear around the threshold energy. First, we show that the three ^8He configuration with the equilateral triangular configuration covers the model space of the lowest shell-model. The expectation value for the principal quantum number

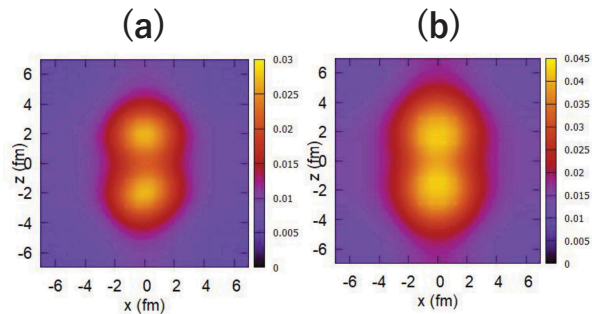


FIG. 5. Intrinsic density of ${}^9\text{Li}$ - ${}^9\text{Li}$ with the relative distance of 4 fm on the xz -plane (fm^{-3}). (a): protons, (b): neutrons.

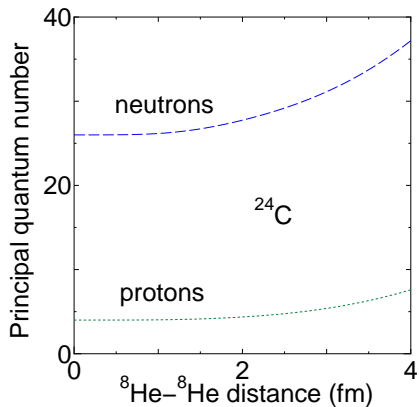


FIG. 6. Expectation value for the principal quantum number of the harmonic oscillator for the 0^+ state of ${}^{24}\text{C}$ with the equilateral triangular configuration of three ${}^8\text{He}$ clusters as a function of the distance between two ${}^8\text{He}$ clusters. Dotted and dashed lines correspond to the result for the protons and neutrons, respectively.

of the harmonic oscillator for the 0^+ state of ${}^{24}\text{C}$ with the equilateral triangular configuration of three ${}^8\text{He}$ clusters is shown in Fig. 6 as a function of the distance between two ${}^8\text{He}$ clusters. Here the dotted and dashed lines represent the results for the protons and neutrons, respectively. They converge to 4 and 26 at small relative distances, respectively. These values are ones for the lowest shell-model configuration; for the protons, two are in the lowest $0s$ -shell and four are in the p -shell ($4 \times 1 = 4$), and for the neutrons, two are in the lowest $0s$ -shell, six are in the p -shell, and ten and in the sd -shell ($6 \times 1 + 10 \times 2 = 26$). Therefore, surprisingly enough, the lowest shell-model configuration of ${}^{24}\text{C}$ is included within the three- ${}^8\text{He}$ model with an equilateral triangular configuration. However, experimentally, the three- ${}^8\text{He}$ threshold is located quite high (more than $E_x = 25$ MeV) in the excitation energy, thus the three- ${}^8\text{He}$ configuration corresponds to a highly excited state.

In Fig. 7, the energy curves of ${}^{24}\text{C}$ with the equilateral triangular configuration of three ${}^8\text{He}$ clusters measured from the three- ${}^8\text{He}$ threshold are shown as a function

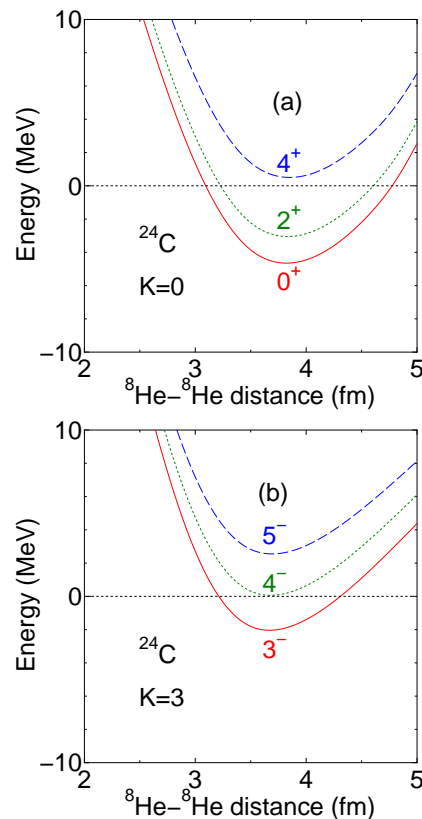


FIG. 7. Energy curves of ${}^{24}\text{C}$ with the equilateral triangular configuration of three ${}^8\text{He}$ clusters measured from the three- ${}^8\text{He}$ threshold as a function of the distance between two ${}^8\text{He}$ clusters. (a): positive-parity $K = 0$ (0^+ , 2^+ , and 4^+), and (b): negative-parity $K = 3$ (3^- , 4^- , and 5^-).

of the distance between two ${}^8\text{He}$ clusters. Here Fig. 7(a) displays the result for the positive-parity states with $K = 0$ (0^+ , 2^+ , and 4^+), and those for the negative-parity states with $K = 3$ (3^- , 4^- , and 5^-) can be found in Fig. 7(b). We can see that both bands appear around the three- ${}^8\text{He}$ threshold energy with large relative distance.

It has been known that if the system has the equilateral triangular configuration (D_{3h} symmetry), both $K = 0$ (0^+ , 2^+ , 4^+ ...) and $K = 3$ (3^- , 4^- , 5^- ...) rotational bands are possible. The appearance of these rotational bands has been extensively discussed in ${}^{12}\text{C}$ [35], which is the signature of the equilateral triangular symmetry of the three α clusters. Now the α clusters are replaced with the ${}^8\text{He}$ clusters and what we discuss here is considered to be the neutron-rich version of the D_{3h} symmetry.

The energy eigen states of the three- ${}^8\text{He}$ cluster states are obtained by superposing the Slater determinants with different relative distances and diagonalizing the Hamiltonian based on the generator coordinate method (GCM). The rotational band structure of three- ${}^8\text{He}$ configuration is shown in Fig. 8, where the solid and dashed lines correspond to the result for $K = 0$ (positive-parity, 0^+ , 2^+ , 4^+ ...) and $K = 3$ (negative parity, 3^- , 4^- , 5^- ...) bands, respectively. Two rotational band struc-

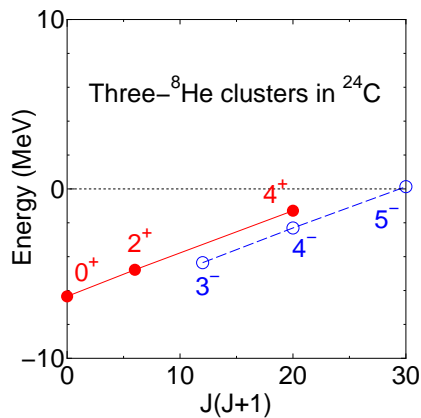


FIG. 8. Rotational band structure of three- ^8He configuration. Solid and dashed lines are the results for the $K = 0$ (positive-parity, 0^+ , 2^+ , 4^+ ...) and $K = 3$ (negative parity, 3^- , 4^- , 5^- ...) bands, respectively.

tures appear around the threshold energy and they have similar slopes as a function of $J(J+1)$.

IV. CONCLUSIONS

Most of the conventional clusters, so far investigated, have been limited to the closure of the three-dimensional harmonic oscillator, such as ^4He , ^{16}O , and ^{40}Ca . Here we discussed the possibility that nuclei with the neutron number six, which is the subclosure of the $p_{3/2}$ sub-shell of the jj -coupling shell model, can be clusters; the ^8He and ^9Li cluster structures have been investigated in ^{16}Be ($^8\text{He}+^8\text{He}$), ^{17}B ($^8\text{He}+^9\text{Li}$), ^{18}C ($^9\text{Li}+^9\text{Li}$), and ^{24}C ($^8\text{He}+^8\text{He}+^8\text{He}$).

We have shown that the lowest principal quantum numbers of ^{16}Be , ^{17}B , ^{18}C , and ^{24}C can be covered within this model. We have just adopted Tohsaki interaction,

which has finite-range three-body terms, and there is no adjustable parameter in the Hamiltonian. Nevertheless the optimal energies of these nuclei measured from the corresponding threshold energies are fairly close to the experimental values. By orthogonalizing the wave functions to the lowest states, very developed cluster states were obtained around the corresponding threshold energies in ^{17}B and ^{18}C .

The appearance of $K = 0$ (0^+ , 2^+ , 4^+ ...) and $K = 3$ (3^- , 4^- , 5^- ...) rotational bands has been extensively discussed in ^{12}C [35], which is the proof for the equilateral triangular symmetry of the three α clusters. In this study, we have replaced the α clusters with the ^8He clusters and shown the neutron-rich version of the rotational band structures for the configuration reflecting the D_{3h} symmetry. The energy eigen states of the three- ^8He cluster states are obtained by superposing the Slater determinants with different relative distances and diagonalizing the Hamiltonian. The two rotational band structures of three- ^8He configuration appear around the threshold energy and they have similar slopes as a function of $J(J+1)$.

As future works, the appearance of the molecular-orbital structure will be studied by adding neutrons to the developed cluster states obtained here in ^{17}B and ^{18}C . Also, we investigate the role of the obtained cluster states, including resonances above the cluster emission threshold around the Gamow window, in the nuclear reactions including the Big Bang nucleosynthesis.

ACKNOWLEDGMENTS

The authors would like to thank fruitful discussions with Dr. Masaki Sasano (RIKEN). The numerical calculations have been performed using the computer facility of Yukawa Institute for Theoretical Physics, Kyoto University.

-
- [1] D. M. Brink, Proc. Int. School Phys. "Enrico Fermi" **XXXVI**, 247 (1966).
[2] M. Freer, H. Horiuchi, Y. Kanada-En'yo, D. Lee, and U.-G. Meißner, Rev. Mod. Phys. **90**, 035004 (2018).
[3] Y. Fujiwara, H. Horiuchi, K. Ikeda, M. Kamimura, K. Katō, Y. Suzuki, and E. Uegaki, Progress of Theoretical Physics Supplement **68**, 29 (1980).
[4] F. Hoyle, Astrophys. J. Suppl. , 121 (1954).
[5] M. G. Mayer and H. G. Jensen, "Elementary theory of nuclear shell structure", John Wiley, Sons, New York, Chapman, Hall, London (1955).
[6] N. Itagaki, S. Aoyama, S. Okabe, and K. Ikeda, Phys. Rev. C **70**, 054307 (2004).
[7] N. Itagaki, A. V. Afanasjev, and D. Ray, Phys. Rev. C **101**, 034304 (2020).
[8] N. Itagaki and S. Okabe, Phys. Rev. C **61**, 044306 (2000).
[9] N. Itagaki, S. Okabe, and K. Ikeda, Phys. Rev. C **62**, 034301 (2000).
[10] N. Itagaki, S. Hirose, T. Otsuka, S. Okabe, and K. Ikeda, Phys. Rev. C **65**, 044302 (2002).
[11] N. Itagaki, M. Ito, M. Milin, T. Hashimoto, H. Ishiyama, and H. Miyatake, Phys. Rev. C **77**, 067301 (2008).
[12] M. Ito and N. Itagaki, Phys. Rev. C **78**, 011602 (2008).
[13] M. Ito, N. Itagaki, and K. Ikeda, Phys. Rev. C **85**, 014302 (2012).
[14] P. Descouvemont and N. Itagaki, Progress of Theoretical and Experimental Physics **2020** (2020), 023D02.
[15] M. Ito, N. Itagaki, H. Sakurai, and K. Ikeda, Phys. Rev. Lett. **100**, 182502 (2008).
[16] M. Ito, Phys. Rev. C **85**, 044308 (2012).
[17] M. Ito, EPJ Web of Conferences **122**, 09002 (2016).
[18] S. Aoyama, N. Itagaki, and M. Oi, Phys. Rev. C **74**, 017307 (2006).
[19] N. Itagaki, M. Ito, K. Arai, S. Aoyama, and T. Kokalova, Phys. Rev. C **78**, 017306 (2008).

- [20] H. Esbensen and G. Bertsch, Nuclear Physics A **542**, 310 (1992).
- [21] Y. Kanada-En'yo and H. Horiuchi, Phys. Rev. C **52**, 647 (1995).
- [22] N. Itagaki, Phys. Rev. C **94**, 064324 (2016).
- [23] N. Itagaki, H. Masui, M. Ito, S. Aoyama, and K. Ikeda, Phys. Rev. C **73**, 034310 (2006).
- [24] H. Masui and N. Itagaki, Phys. Rev. C **75**, 054309 (2007).
- [25] T. Yoshida, N. Itagaki, and T. Otsuka, Phys. Rev. C **79**, 034308 (2009).
- [26] N. Itagaki, J. Cseh, and M. Płoszajczak, Phys. Rev. C **83**, 014302 (2011).
- [27] T. Suhara, N. Itagaki, J. Cseh, and M. Płoszajczak, Phys. Rev. C **87**, 054334 (2013).
- [28] N. Itagaki, H. Matsuno, and T. Suhara, Progress of Theoretical and Experimental Physics **2016**, 093D01 (2016).
- [29] H. Matsuno, N. Itagaki, T. Ichikawa, Y. Yoshida, and Y. Kanada-En'yo, Prog. Theor. Exp. Phys. **2017**, 063D01 (2017).
- [30] H. Matsuno and N. Itagaki, Progress of Theoretical and Experimental Physics **2017**, 123D05 (2017).
- [31] N. Itagaki and A. Tohsaki, Phys. Rev. C **97**, 014307 (2018).
- [32] N. Itagaki, H. Matsuno, and A. Tohsaki, Phys. Rev. C **98**, 044306 (2018).
- [33] A. Tohsaki, Phys. Rev. C **49**, 1814 (1994).
- [34] R. Tamagaki, Progress of Theoretical Physics **39**, 91 (1968).
- [35] D. J. Marín-Lámbbarri, R. Bijker, M. Freer, M. Gai, T. Kokalova, D. J. Parker, and C. Wheldon, Phys. Rev. Lett. **113**, 012502 (2014).